Mussel Byssus-Like Reversible Metal-Chelated Supramolecular Complex Used for Dynamic Cellular Surface Engineering and Imaging

*Wen Li, Wei Bing, Sa Huang, Jinsong Ren, and Xiaogang Qu**

Inspired by the load-bearing biostructures in nature, a multifunctional shell for encapsulating cell using the polyphenol–metal complexes is fabricated. The artificial shell is formed by cross-linking of tannic acid and iron ion on cell surface. It can protect cells from unfriendly environments, including UV light irradiation and reactive oxygen damage. With the hybrid property of polyphenol and metal liands, the shell provides a versatile platform for cell surface engineering. The magnetic nanoparticles, DNA molecules, as well as the magnetic resonance imaging agents are easily incorporated into the shell. More interestingly, unlike the traditional passive coatings, here the shell can be controllably disassembled under external stimuli. The dynamic coating is used as a reversible element to regulate cell division and surface modification. The cell viability and protein expression experiments further confirm that the shell formation and degradation processes are biocompatible. This multifunctional coating strategy is applicable to multiple living cell types, including yeast cells, *Escherichia coli* bacteria, and mammalian cells. Therefore, this platform would be useful for living cell based fundamental research and biological applications.

1. Introduction

For cell-based applications, such as bioelectronic devices, biocatalysis, cell-based sensors, and therapies,[1–5] it is of scientific interest and technological importance for long-term cell viability and functionality in unfriendly environments.[6–9] All these issues have inspired the strategies to protect cells against physical, chemical, or biological stress. Engineering cell surface with appropriately designed materials is well poised to address such challenges and also provides powerful tools for regulating cellular functions.[10–17] In the past few years, a number of approaches have been devised for engineering cell surface.[18–22] As the advanced molecular biology techniques, genetic and metabolic approaches have been explored to program cell surface to express receptors or glycoproteins.[19] Although clever, they may be restricted to the natural canon of available biochemical pathways. Covalent conjugation with membrane protein or incorporation of phospholipids into cell membranes is also used for cell surface modification.[20] However, they may perturb cell membrane function in undesired manners. Recently, the layer-by-layer assembly of polyelectrolytes has emerged as a valuable method for cell surface engineering.[10] The nanoshells not only provide mechanical support for cells but also allow efficient transport of nutrients. Nevertheless, the cytotoxicity elicited by most polycations is a major obstacle of polyelectrolyte film. In addition, most of the engineering strategies are not reversible and play a permanent and uncontrolled role in cells. It holds numerous advantages to fabricate a versatile and dynamic shell that can initially protect and regulate cells and then can be on-demand removed to evoke the original property of cells.

Nature has long been a source of inspiration for material science.[23–26] Recently, the metal–polymer complex has aroused much attention due to its wide distribution in nature, especially in certain load-bearing biostructures.[27–33] Formed by cross-linking of polymer with metal ligand, the coordination complexes endow biological structures with many desirable properties, such as adhesion, self-assembly, self-repair, mechanical tunability and toughness.[34–37] For example, the histidine–zinc complexes are correlated to the hardness of the jaws of marine worms.[34] Additionally, the byssal cuticle of mussel exhibits a peculiar combination of high stiffness and extensibility, which can shield the byssal threads from abrasion. Recent studies confirmed that multivalent catecholato–iron complexes played an integral role in this unique mechanical property.[35,36] Inspired by the excellent performance of metal–polymer complex in biostructures, we described a versatile strategy to encapsulate cells using the polyphenolic metal complex-based shell

Dr. W. Li, Dr. W. Bing, Prof. J. Ren, Prof. X. Qu
Laboratory of Chemical Biology and
State Key Laboratory of Rare Earth Resource Utilization
Changchun Institute of Applied Chemistry
Chinese Academy of Sciences
Changchun, Jilin 130022, China
E-mail: xqu@ciac.ac.cn
Dr. W. Li, Dr .W. Bing, Prof. J. Ren, Prof. X. Qu
University of Chinese Academy of Sciences
Beijing 100039, China
Dr. S. Huang
Department of Radiology
The Second Hospital of Jilin University
Changchun, Jilin 130041, China

DOI: 10.1002/adfm.201500039

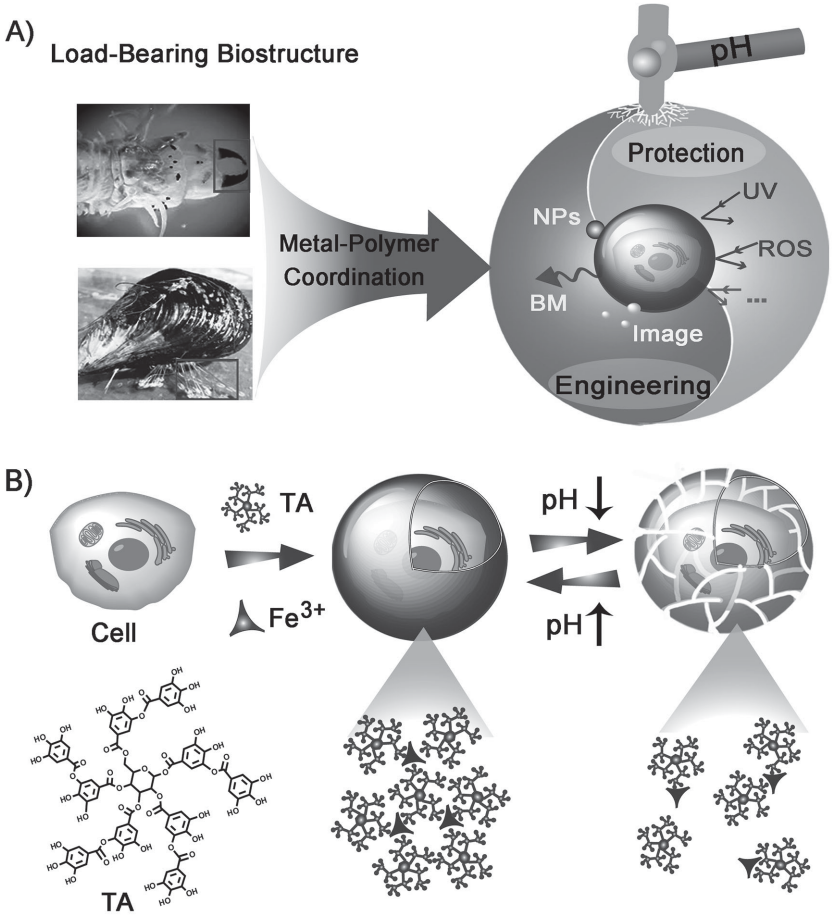

Figure 1. A) Inspired by the widespread metal–polymer complexes in the load-bearing biostructures, such as the jaws of marine worms and the byssal cuticle of marine mussels, a versatile approach for encapsulating cells was developed with polyphenol–metal complexes. The shell could protect cells from UV irradiation and oxidative stress. It also provided a convenient route to modify cell surface with nanoparticles (NPs), bioactive molecules (BM), image reagent. B) The encapsulation of cells with shells through sequential addition of tannic acid (TA) and Fe^{3+} and the reversible removal of the shell through the acid trigger.

(**Figure 1**). First, the cross-linking process of polyphenol and metal was rapid. It did not involve the laborious processes or the exposure to toxic reagents.[35,36] This provided a simple and biocomparable coating strategy. Second, the hybrid properties of polyphenols and metals endowed the shell with multifunctions. The polyphenols displayed a broad cellular protectability including absorption of UV light and radical scavenging,[38,39] and they also showed chemical reactivity toward nucleophilic groups.[38–44] When it came to metal ligands, a wide range of metals with unique optical or magnetic properties were capable of forming coordination complex with polyphenols.[45] Accordingly, the shell designed here provided a versatile platform to modify cell surface with nanoparticles, bioactive molecules, as well as imaging contrast agents. It is, however, usually difficult for the existing examples to modify cell surface with multiple classes of functional materials conveniently. Last, but not least, a robust but dynamic coating strategy is very essential for on-demand regulation of cells, but is still challenging. The covalent methods have proven to be highly stable, but they are usually not reversible. The noncovalent approaches such as the hydrogen-bonded layer-by-layer coating possess high tunability but they do not permit long-term stability. In our strategy, the multidentate complexes between polyphenol and metal (such as iron) exhibited not only the near covalent stability but also the stimuli-responsive property. Upon the decrease of pH, the coordination stoichiometry of polyphenol and metal was changed,[45–48] which resulted in the reversible disassembly of the coating. In this sense, the shell could initially support the protection, regulation, and track of cells. While, after completing its role, the artificial coating could be controllably removed with stimuli to release the cells and reactivate the cellular functions. The on-demand coating strategy will be critically important for highly sensitive biosensing and active cell manipulation.

2. Results and Discussion

As the low-cost and readily available substitute for mussel polyphenolic protein, plant polyphenol tannic acid (TA) was chosen as the polymer ligand to coordinate with Fe^{3+}. To illustrate the versatility of our strategy, we first described the assembly of TA–Fe^{3+}-based shell on yeast cell as it is a popular system for understanding eukaryotic cell.[49,50] The yeast cells were readily coated with the coordination-based shells through sequential addition of TA and Fe^{3+} to cells suspension. Each iron ion center could bind three galloyl groups of TA, resulting in the cross-linking of TA and Fe^{3+} on cell surface. As shown in Figure S1 (Supporting Information), upon addition of TA and Fe^{3+}, the yeast cell suspension immediately turned blue. The opacity change was attributed to the formation of TA–Fe^{3+} complexes. Prolonging the reaction time from 30 s to 30 min had little effect on the cell color. This indicated that the film could be formed on cell surface within minute. The efficiency of the coating process was studied in more detail (Figures S2–S4, Supporting Information). Successful assembly of the shells was confirmed by zeta-potential with the cell surface potential changed from –16.9 to –30 mV (Table S1, Supporting Information). The shell-coated cells were then studied with scanning electron microscopy (SEM) images. As shown in Figure S5 (Supporting Information), the bare cells were obviously shrunk because of dehydration, whereas yeast cells at TA–Fe^{3+} were typically round-shaped. The magnified image indicated that the cell surface became rough after coating (**Figure 2**a,b). Transmission electron microscopy (TEM) images (Figure 2c–f) further showed that the average thickness of shell was about 40 nm and the thickness increased with the coating cycles (Figure S6, Supporting Information). As a derivative of marine protein adhesives, TA exhibits strong adherence activity

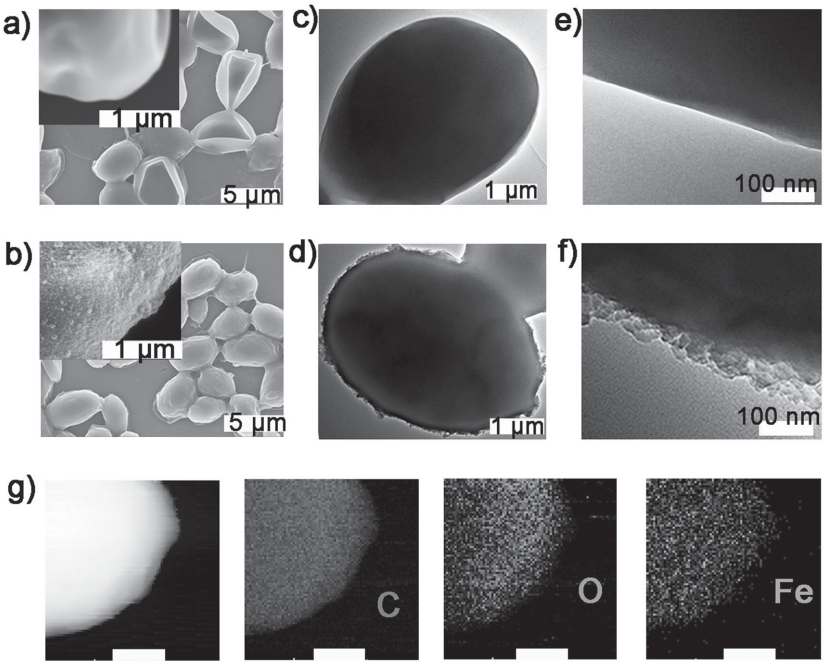

Figure 2. SEM images of a) the bare yeast cells and b) the yeast cells with TA–Fe^{3+} shell. Insets were the magnified images of the corresponding yeast cell surface. TEM images of bare yeast cells c,e) and the yeast cells with TA–Fe^{3+} shell d,f) with different magnifications. g) EDX elemental mapping of TA–Fe^{3+} shell on yeast cell surface. From left to right were the high angle annular dark-field (HAADF) image of the part of a yeast cell, and the corresponding elemental mappings of the C K-edge, O K-edge, and Fe K-edge signals. The scale bars were 0.5 μm.

for a wide range of interfaces.[38–40] Thus, it was most likely that the free TA initially adsorbed onto cell surface. Then, it could be cross-linked by forming octahedral complex with Fe^{3+}. The further increase of Fe^{3+} may draw more TA and small TA–Fe^{3+} complexes to the initially formed films (Figure S7, Supporting Information). As shown in the SEM image (Figure S8, Supporting Information), the increase of Fe^{3+} concentration made the shell thicker and rougher, which indicated that Fe^{3+} played a central role in the cross-linking process. The energy-dispersive X-ray (EDX) spectroscopy indicated the presence of Fe element on the shell (Figure S9, Supporting Information). The elemental mapping analysis (Figures 2g and S10, Supporting Information) further demonstrated that the distribution patterns of Fe element matched well with those of C and O elements, as well as the high angle annular dark-field images (HAADF) of cell. This proved that the TA–Fe^{3+} shell was well distributed on cell surface and the cell inside was not obviously shrunk.

It was critical to investigate the physiological effect of shell on cells. The survival of the enclosed cell was studied with live/dead staining assay based on calcein-AM (AM) and propidium iodide (PI). AM can be deacetylated by the esterase of living cells and releases a green fluorescent molecule, while the red fluorescent molecule PI can enter only nonviable cells to stain nucleic acids of dead cells. As shown in **Figure 3**a, the viability of the coated cells was about 95%, which was similar to that of bare cells. It was notable that the shell did not prevent PI from entering dead cells. For control cells that were killed by ethanol or heating, the coating with shell did not influence the staining results (Figure S11, Supporting Information). The high cell viability was originated from the mild coating process and the low toxicity of shell. Next, we studied whether the shells could protect cells and stabilize cell viability for long term. For bare cells, they nearly lost all their viability in water within 15 d. However, about 70% of the coated cells were still alive at the same time point (Figure 3b). This demonstrated that the shell could prolong cell viability. In addition, TA displayed diverse biological functions such as structural support, UV light absorption, and radical scavenging.[38,39] These features might endow the shells with special protective effects. As expected, after exposure to UV light, the viability of the coated cells was exactly higher than that of bare cells (Figure 3c). The radical scavenging property of the shell was also probed. As monitored by flow cytometry, the intracellular reactive oxygen species (ROS) levels were attenuated in the presence of shell (Figure S12, Supporting Information). Following the protection assay, we examined the influence of shell on cell division. While native yeast cells immediately proliferated into exponential phase after 3 h,[49] the growth of shell-coated cells exhibited an obvious delay (Figure 3d). The delay of cell division was dependent on the thickness of shell, but the cells still kept the capability of dividing themselves (Figure S13, Supporting Information). The result showed that the shell could be utilized to control the cell division cycles in a designed way.

Cell-surface modification is another important issue for the applications of living cells.[18–21] So far, it is still challenging to find a versatile platform to modify cell surface with multiple functional materials. As reported previously, polyphenols not only displayed high affinity with metals and metal oxides but also supported chemical reactions with nucleophilic groups.[38–44] Thus, the TA–Fe^{3+} shell would provide a convenient route for cell surface modification. The magnetic modification of individual living cell was first performed by mixing the magnetic nanoparticles (MNPs) with the shell-coated cells as TA could bind MNPs strongly via COFe bond.[51–54] The successful binding of MNPs on the cell surface was verified by the on-demand collection and release of cells with magnetic field (**Figure 4**a). The cells were further assembled into arrays by magnets. This indicated the potential use for separation, immobilization, and delivery of cells. In addition to nanoparticles, the shells also supported the covalent conjugation of biomolecules via the chemical reactivity of polyphenols toward amine or thiol groups.[38–44] DNA with amine terminus was grafted to the coated cell surface to endow cell with biorecognition. The modified cells were specially immobilized on the complementary DNA-presenting glass substrate (Figure 4b). For control, the cells without DNA modification exhibited negligible interaction with the same surface. What is more, the coordination-based

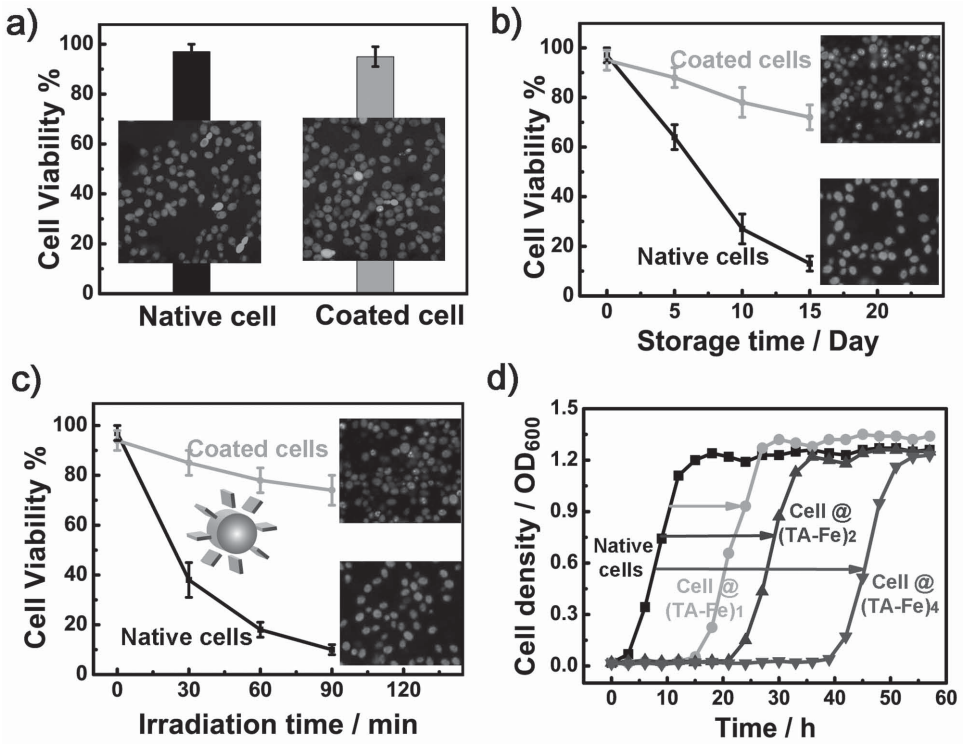

Figure 3. a) The live/dead fluorescence images and the corresponding viability analysis of native yeast cells and the shell-coated yeast cells. b) The viability of native yeast cells and shell-coated yeast cells in water against time. Insets were the live/dead fluorescence images of the corresponding yeast cells after storage for 15 d. c) The viability of native yeast cells (black) and shell-coated yeast cells after irradiation with UV light for different times. Insets were the fluorescence images of corresponding yeast cells after exposure to UV light for 90 min. d) Growth curve of native yeast cells, yeast cells at $(TA–Fe^{3+})_1$, yeast cells at $(TA–Fe^{3+})_2$, and yeast cells at $(TA–Fe^{3+})_4$. The error bars represented the standard deviation of three experiments.

shells were not limited to the use of Fe^{3+} as ligand. Many metal ions, such as aluminum, manganese, titanium, zirconium, molybdenum, cerium, europium, and gadolinium, were capable of forming complexes with polyphenols.[34,45,46] By incorporating single or multiple metals, a diverse range of functional shells could be generated. As an example, we explored the incorporation of magnetic resonance image (MRI) contrast agents to the shell by cross-linking of TA with Fe^{3+}, Mn^{2+}, and Gd^{3+}. MRI has been regarded as a powerful analytical tool in biomedical field for its high sensitivity, high spatial resolutions, and large penetration depth.[55–58] The T1-weighted MR images of the coated cells were evaluated with a 3.0 T human clinical scanner. As shown in Figure 4c, the MR signals were enhanced with the increase of the coated cell concentration for all the three samples. This provided a noninvasive image method for cells, which would be beneficial for monitoring cell fate and fabricating cell-based sensors.

Next, we investigated whether the shell had a dynamic nature, which was highly important for on-demand manipulation of cell growth kinetics and surface engineering. Upon incubation in an acidic media, the original inert cells at $TA–Fe^{3+}$ were reactivated and switched to dividing mode (**Figure 5**a). For control, the growth of bare cells was not obviously affected by the slightly acid pH (Figure S14, Supporting Information). The dramatic change in the growth mode of the encapsulated cells was associated with pH-triggered structural change of shells. At low pH, the hydroxyl groups of TA were protonated and their coordination stoichiometry with Fe^{3+} was changed from tris- to bis- to mono-coordinated state.[45–47] This was accompanied with the rapid disassembly of the shell (Figure 5b). Beside pH, ethylenediaminetetraacetic acid (EDTA) also accelerated the degradation because of its strong affinity with Fe^{3+}. As shown in Figure 5c, the shells on cell surface became thinner and partly disappeared under stimuli, which resulted in the release of cells from coating. The degradation of $TA–Fe^{3+}$-based cross-links with stimuli was also confirmed by atomic force microscope (AFM). From Figure S15 (Supporting Information), we could see that the $TA–Fe^{3+}$ film on the flat surface became thinner after pH and EDTA treatment. It should be noted that these stimuli processes did not affect cell viability (Figure S16, Supporting Information). The growth curves of the reactivated cells were almost same as that of native cells (Figure 5a). After removing the shell by acid or EDTA treatment, the cell viability was also studied with live/dead staining (**Figure 6**a). The quantitative analysis showed that more than 85% cells were still alive (Figure 6b). In addition, the cells were reincubated on the yeast–extract–peptone–dextrose (YPD) agar plate overnight (Figure 6c). Compared with the native cells, only a few of colonies were formed for the shell-coated cells due to the suppression of cell division by shell. While, after the disassembly of shell by stimuli, the proliferation ability of cells was restored and the colony numbers of the released cells were similar to that of native cells. This implied that the activity of living cells was not obviously affected by the encapsulation and the release

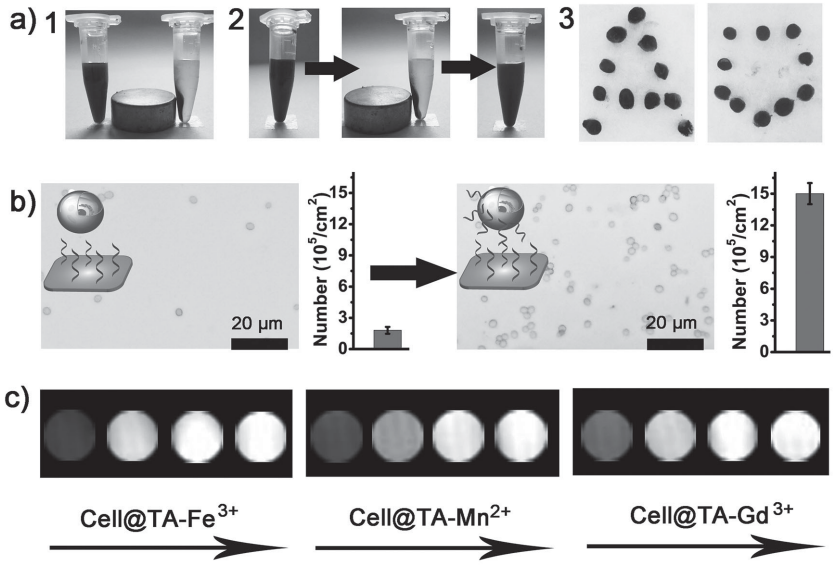

Figure 4. a) (1) Compared with the control yeast cells without magnetic modification (left), the magnetically modified yeast cells at TA–Fe^{3+} (right) could be quickly collected by a magnet. (2) The reversible collection and release of magnetic yeast cells by the contact or removal of magnetic force. (3) The assembly of magnetic yeast cells to the pattern of "A" and pentagon with magnetic force. b) The optical image and the number of yeast cells at TA–Fe^{3+} (as control, left) and DNA-linked yeast cells at TA–Fe^{3+} (right) cultured on the complementary DNA-presenting substrate. The scale bars were 20 μm. c) T1-weighted MRI images of the yeast cells at TA–Fe^{3+}, yeast cells at TA–Mn^{2+}, and yeast cells at TA-Gd^{3+}. For each sample, the concentrations of the coated yeast cells from left to right were 0, 10, 20, 50 mg mL^{-1}. The error bars represented the standard deviation of three experiments.

process. Beside the growth kinetics, the surface engineering of cells could also be reversibly regulated by the dynamic shell. Upon incubation in the acid solution, the magnetically modified cells lost their response toward magnetic field because the magnetic nanoparticles were removed along with the shell (Figure S17, Supporting Information). When it came to the DNA-linked cells, the pH stimulus also resulted in the abatement of their special interaction with the complementary DNA-presenting substrate (Figure 6d). In addition, the T1-weighted MR signal of the coated cells also greatly decreased after removing the TA–Fe^{3+} shell with triggers (Figure 6e).

To show the versatility of the coating, this strategy was further applied to *Escherichia coli* bacteria. As the very common bacterium in biotechnology, *E. coli* shows wide applications in molecular cloning, proteins express, and protein function testing. The morphology of *E. coli* at TA–Fe^{3+} was studied by SEM images. As shown in **Figure 7**b, the shell-supported cells were typically rod-shaped, while the native cells were seriously shrunk and wrinkled (Figure 7a). From the magnified SEM image, we could see that the surface of the coated cells become rough. The TEM image further confirmed the shell was uniformly formed on the *E. coli* surface (Figure S18, Supporting Information). The EDX spectroscopy further confirmed the successful coating with the Fe element peak at 6.40 keV. The cell viability analysis obtained from live/dead staining assay implied that about 94% cells were still alive after the coating process (Figure 7c). Beyond viability, the function activity of cells was also evaluated by their ability to produce fluorescent protein in an inducer-responsive manner. A significant fluorescence emission was observed for both the control and the shell-coated cells in the presence of inducer (Figure 7d). As monitored by flow cytometry (Figure 7e,f), the fluorescent intensity of the shell-coated cells was similar to that of native cells. The results confirmed that the encapsulation did not adversely influence the fluorescent protein expression of cells. The protective ability of the shell was studied by UV light irradiation experiment. As shown in Figure S19 (Supporting Information), the resistance of *E. coli* to UV light greatly increased in the presence of shell. After the degradation of the shell by stimuli, the solution color of the coated cells was gradually changed from blue to white. The acid and EDTA stimuli used in our experiments were biocompatible to the *E. coli* bacteria (Figure S20, Supporting Information). Importantly, the cell viability did not decrease significantly during the stimuli. And the fluorescent protein express ability of the shell-removed cells was also maintained. The results were consistent with those of yeast

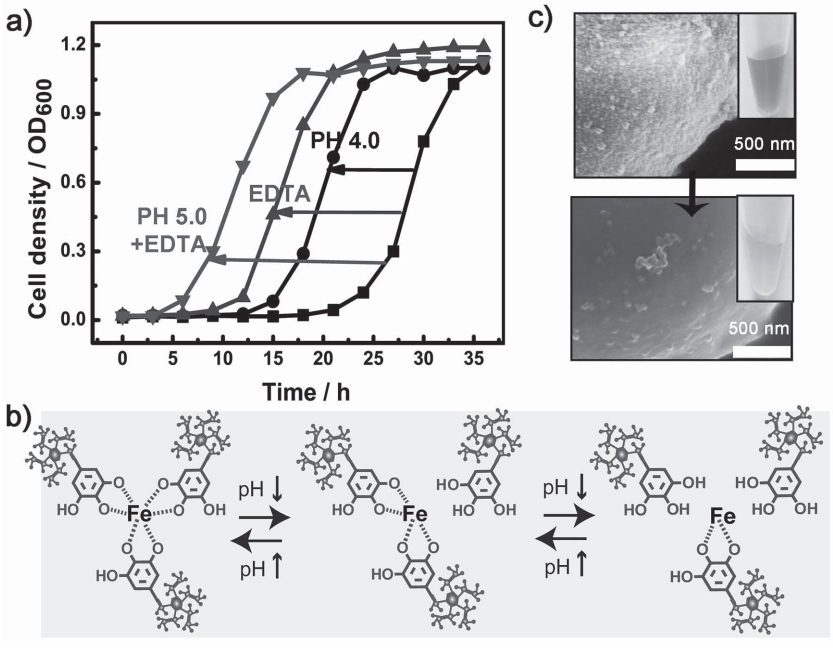

Figure 5. a) Growth curve of yeast cells at $[TA–Fe^{3+}]_2$ before and after stimulation with pH 4.0, EDTA, and pH 5.0 + EDTA. b) The pH-dependent stoichiometry change of TA–Fe^{3+} complexes. c) SEM images showed the surface of the coated yeast cells before (up) and after stimuli (down). The photographs inserted showed the color changes of the coated yeast cell solution.

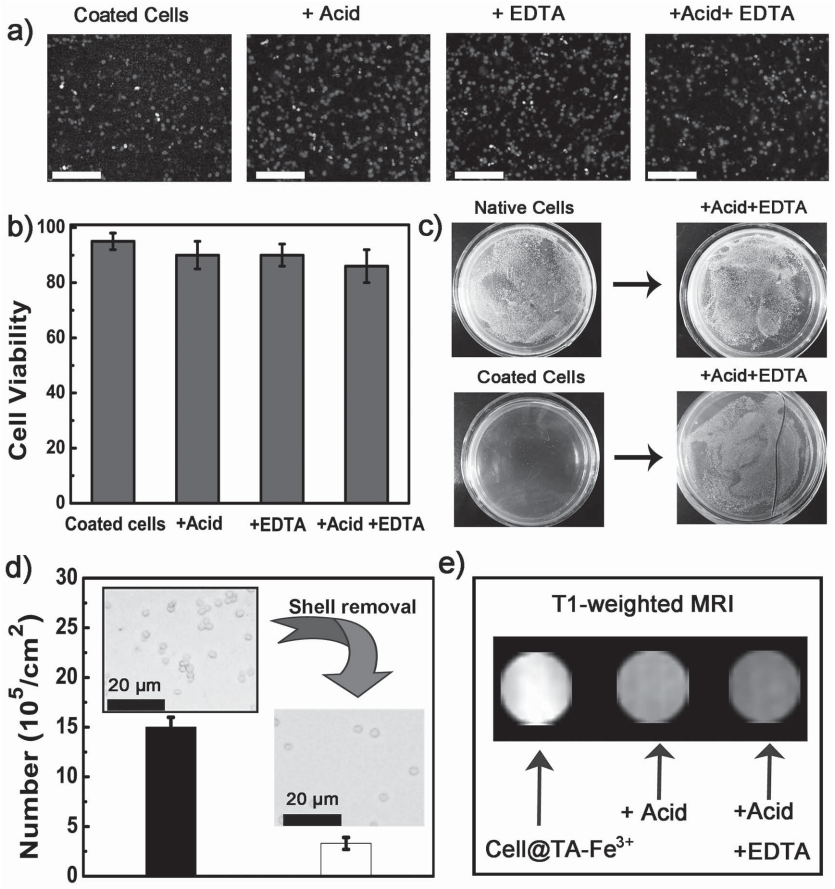

Figure 6. a) The live/dead fluorescence images of yeast cells before and after removal of shell by acid (pH 4.0), EDTA, or acid + EDTA. The scale bars were 50 μm. b) The quantitative viability analysis of yeast cells before and after degrading the shell by stimuli. c) Representative digital images showed the grown colonies of yeast cells on agar plates. For this, the native yeast cells before and after acid + EDTA treatment (top row) and the shell-coated yeast cells before and after acid + EDTA treatment (second row) were cultured on the agar plates overnight. d) The number of DNA-linked yeast cells at TA–Fe^{3+} immobilized on the complementary DNA-presenting substrate. After the removal of shell by acid, the yeast cells immobilized on the same surface decreased. Insets were the corresponding optimal image of yeast cells on surface. The scale bars were 20 μm. e) The T1-weighted MR signal of the yeast cells at TA–Fe^{3+}, and the coated yeast cells after acid and acid + EDTA treatment. The error bars represented the standard deviation of three experiments.

cells, which implied that the shell coating and removing process were cytocompatible and had negligible effect on the cell activities and viability. The encapsulation system was also explored to the PC-12 cells, one kind of mammalian cell (**Figure 8**). After coated with the shells, the PC-12 cells still had high viability and their resistance to UV light was greatly enhanced.

3. Conclusion

In summary, inspired by the widespread metal–polymer complexes in the load-bearing biostructures of nature, here we described a facile and versatile approach for encapsulating and engineering cells by using polyphenol–metal complexes. The shell could prolong cell viability and protect cell from UV light radiation and reactive oxygen damage. It also provided a powerful tool for modifying cell surface with nanoparticles, bioactive molecules, and imaging contrast agents. The broad modification of multiple functional materials on cell surface has not been so conveniently achieved in the existing examples. More interestingly, the coordination-based shell uniquely combined the near covalent stability and stimuli-responsive flexible nature, which provided a robust but dynamic coating to cell. The responsive shell was used as a reversible element to regulate cell division and surface modification. It also should be noted that the shell coating and removing processes were cytocompatible and had negligible effect on cell viability. In this sense, the shell could initially serve as a multifunctional platform for protecting cell, controlling cell interactions, and monitoring cell fate. Then, after completing its role, the coating could be controllably disassembled with stimuli, which facilitated the cell release and reactivated the cell function. The multifunctional and dynamic coating strategy will suggest a promising platform for living cell-based fundamental research and biological applications.

4. Experimental Section

Materials: Tannic acid (TA), iron (III) chloride hexahydrate ($FeCl_3{\cdot}6H_2O$), iron dichloride ($FeCl_2$), manganese chloride tetrahydrate ($MnCl_2{\cdot}4H_2O$), gadolinium nitrate hexahydrate ($Gd(NO_3)_3{\cdot}6H_2O$), sodium cyanoborohydride, and ethylenediaminetetraacetic acid (EDTA) were purchased from Aladdin Reagent (Shanghai, China). (3-Aminopropyl)trimethoxysilane (APTES), 2′,7′-dichlorofluorescein diacetate (DCFH-DA), propidium iodide (PI), and calcein (AM) dye were provided by Sigma-Aldrich. DNA used was synthesized by Sangon Biotechnology Co. (Shanghai, China). Other reagents and solvents were achieved from Beijing Chemicals (Beijing, China). All chemical agents were of analytical grade and used directly without further purification. All aqueous solutions were prepared using ultrapure water (18.2 MU, Milli-Q, Millipore).

Characterizations: UV–vis absorbance measurement was carried out on a JASCO V-550 UV–vis spectrophotometer. The zeta-potential was measured in a Zetasizer 3000HS analyzer and each value of zeta-potential was acquired by averaging three independent measurements. The cells with or without the coating were dispersed in deionized water. The aqueous solution of cells with OD_{600} = 0.3 was used to perform zeta-potential measurements. AFM images were performed using a Nanoscope V multimode atomic force microscope (Veeco Instruments, USA) in tapping mode. Scanning electron microscopic (SEM) images and in suit EDX analysis were recorded using a Hitachi S-4800 Instrument (Japan). Before imaging, cells were air-dried on silicon wafers and sputter-coated with platinum. Transmission electron microscopic (TEM) images were captured with an FEI TECNAI G2 20 high-resolution transmission electron microscope operating at 200 kV. T1-weighted MR imaging was acquired by using a 3.0 T clinical MRI

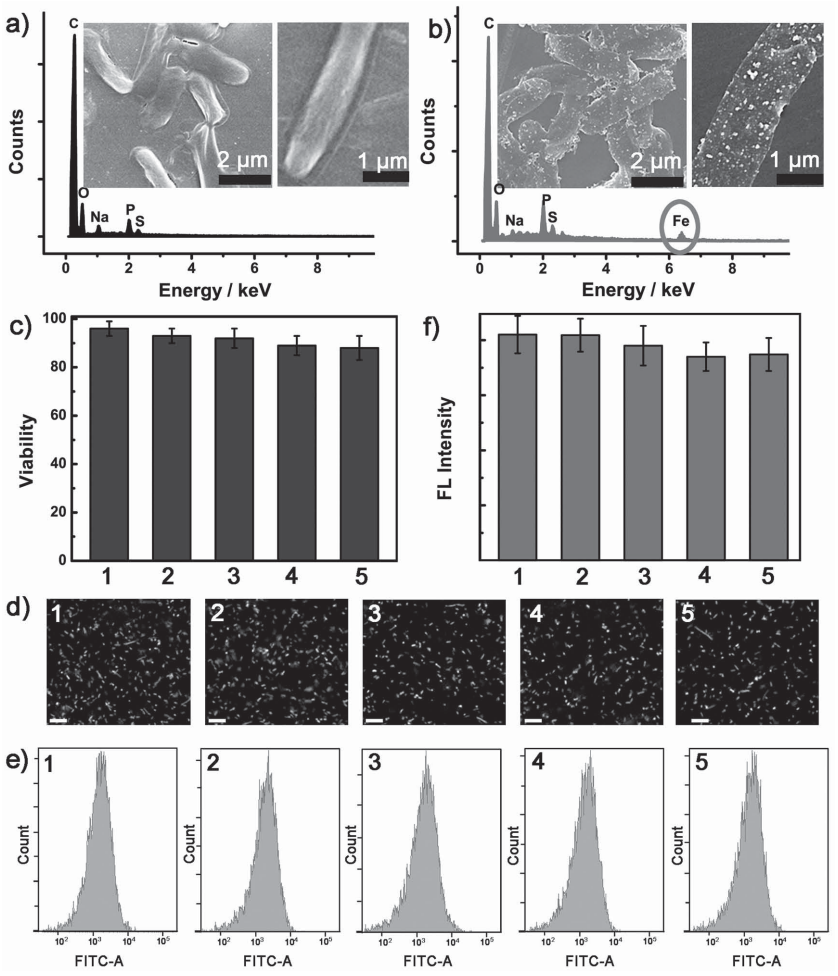

Figure 7. The SEM image, magnified SEM image, and EDX spectrum of a) the native *E. coli* bacteria and b) the *E. coli* bacteria with TA–Fe^{3+} shell. In (c–f), the viability and fluorescent protein express of native *E. coli* bacteria (sample 1), the *E. coli* bacteria at TA–Fe^{3+} (sample 2), the *E. coli* bacteria after removing the shell by acid stimulus (sample 3), EDTA stimulus (sample 4), and acid + EDTA stimulus (sample 5) were analyzed. c) The viability analysis of *E. coli* bacteria obtained from the live/dead staining assay. d) The fluorescence images of *E. coli* bacteria after the induced expression of fluorescent protein. The scale bars were 10 μm. e) Flow cytometry analysis of fluorescent protein expression in *E. coli* bacteria after induction. f) Quantification of fluorescence protein expression in different *E. coli* bacteria obtained from flow cytometry analysis. The error bars represented the standard deviation of three experiments.

instrument (Siemens Medical System). Dilutions of cell at TA–Fe^{3+}, cell at TA–Mn^{2+}, and cell at TA–Gd^{3+} in water with different concentrations were placed in a series of 4.0 mL Eppendorf tubes for T1-weighted MR imaging. After careful preparation, the Eppendorf tubes were then scanned in a 3.0 T Magnetom Espree MIR system.

Encapsulation of Yeast Cells with TA–Fe^{3+}: The yeast cells were suspended in the yeast–extract–peptone–dextrose (YPD) broth and cultured in a shaking incubator at 30 °C with 225 rpm to bring them to an early exponential phase. Then, yeast cells were harvested in 1.5 mL centrifuge tubes by centrifugation at 2000 rpm for 2 min and washed three times in the 0.85% aqueous NaCl solution. Solution of TA and then $FeCl_3{\cdot}6H_2O$ were added to the yeast cell suspension to yield the 1.5 mL solution with 0.5 mmol L^{-1} $FeCl_3{\cdot}6H_2O$ and 0.25 mmol L^{-1} TA. The suspension was mixed by a vortex mixer for 30 s immediately after the individual additions of TA and $FeCl_3{\cdot}6H_2O$. After that, the pH of the suspension was adjusted to neutral pH by buffer. The resulting yeasts were collected with centrifugation and washed with water three times to remove excess TA and $FeCl_3{\cdot}6H_2O$. For multicoating, the assembly step was performed repeatedly to obtain the cells at $(TA–Fe^{3+})_n$, where *n* denotes the number of layers. For the characterization, yeast cells at $[TA–Fe^{3+}]_2$ were used unless noted otherwise. For using other metal ions as ligands, the same concentration of $MnSO_4$ or $GdCl_3$ solution was used to replace the $FeCl_3$ solution. After the sequential addition of TA and $MnSO_4$ or $GdCl_3$ solution, the cell suspension was mixed and centrifuged to obtain the cell at TA–Mn^{2+} or cell at TA–Gd^{3+}.

The Protection Effect of the Shell to Cells: Cell viability of the noncoated and coated cells was assessed with live/dead assay based on propidium iodide (PI) and Calcein-AM (AM). AM was deacetylated by esterase in the cytoplasm of living cell and released a green fluorescent molecule, while the red fluorescent molecule PI can enter only nonviable cells to stain nucleic acids of dead cells. The 2 μL of the stock solution of Calcein-AM (1 mg mL^{-1}) and PI (1 mg mL^{-1}) were mixed with 1 mL of yeast cell suspension. After incubation for 30 min at room temperature while shaking, the cells were collected by centrifugation and were viewed by the Olympus BX-51 optical system microscope (Tokyo, Japan). The micrographs were analyzed with Image J software to quantify the number of live (green) and dead (red) cells. For UV exposure, 24-well plates containing 1 mL of uncoated or coated cell suspension were placed in a biological safety cabinet with the germicidal lamp turned on (30 W G30T8 UV bulb). The bulb emitted short-wave UV radiation centered at 254 nm. At set intervals, plates were removed from the cabinet, and the cell viability was assessed with live/dead assay. The intracellular reactive oxygen radicals (ROS) were monitored using 2′,7′-dichlorofluorescein diacetate (DCFH-DA).[38] After reacting with intracellular ROS, this nonfluorescent dye was changed to a fluorophor, dichloro-fluorescein (DCF). Thus, the DCF fluorescence intensity was related to the amount of intracellular ROS. To perform the test, DCFH-DA solution (20×10^{-3} M) was added to the suspension of bare or shell-coated cells, and the mixture was incubated for 1 h. The cells were then washed twice with PBS and were treated with free-radical initiator. Finally, the fluorescence intensity of the treated cells at 530 nm with excitation at 485 nm was monitored by flow cytometric analysis.

Cell-Division Test: The optical density of bare or coated cells at 600 nm was first adjusted to ≈1.0 by water. Then, 5 μL of the yeast mixture was added to the YPD broth and cultured in a shaking incubator at 30 °C. At indicated time points, the small amount of cells was taken out and its optical density at 600 nm (OD_{600}) was monitored by UV–vis spectroscopy.

Surface Functionalization: For cell surface modification, the cells at TA–Fe^{3+} were first immersed into the TA solution and then were collected by centrifugation for further use. In order to magnetic modification of individual cell, the magnetic nanoparticles (MNPs) were synthesized following the previous work.[59] The 10 μL of 10 mg mL^{-1} MNPs was added to 1 mL of coated cells and the mixtures were gently stirred for 30 min. The MNPs could bind to the shells via coordination bond between iron and oxygen.[51–54] The magnetized cells were separated via centrifugation and a permanent magnet. For conjugation of DNA on the shell-coated cells,[38–43] 20 μL of 100×10^{-6} M DNA with the terminal amine group (DNA 1, its sequence was 5′-GGGTTAGGGTTAGGGTTAGGGTTTTTT-NH2-3′) was added

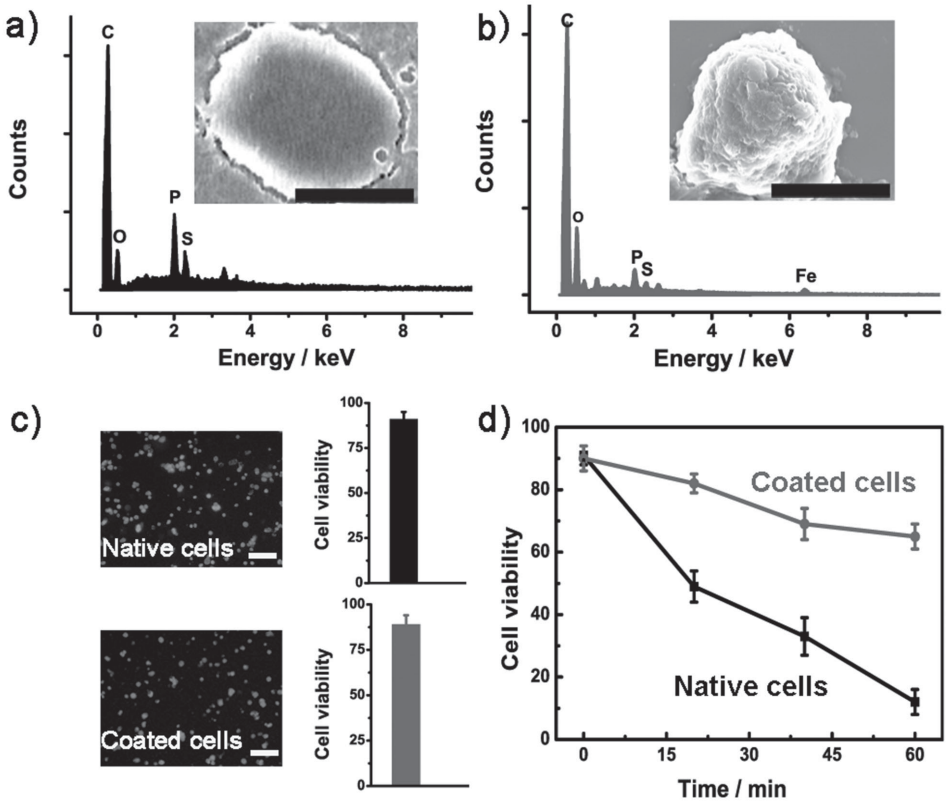

Figure 8. The SEM image and EDX spectrum of the native PC12 cells a) and the PC12 cells with TA–Fe^{3+} shell b). The scale bars were 10 μm. c) The live/dead fluorescence images and the corresponding viability analysis of native PC12 cells (top row) and the shell-coated PC12 cells (second row). The scale bars were 50 μm. d) The viability of native PC12 cells and shell-coated PC12 cells after UV light irradiation for different times. The error bars represented the standard deviation of three experiments.

into the cells at TA–Fe^{3+} suspension and the mixtures were allowed reacting for 3 h with gentle stirring. After removal of unreacted DNA by centrifugation, the DNA-grafted cells were obtained and were then dispersed in PBS buffer. The complementary DNA-presenting glass substrate was prepared as previously described.[60] Briefly, 80×10^{-6} M solution of 3′-amino DNA (DNA 2, its sequence was 5′-CCCTAACCCTAACCCTAACCCTTTTTT-NH2-3′) in pH 7.0 sodium chloride sodium citrate (SSC) buffer was added to aldehyde-coated glass and dehydrated in a 100 °C oven 30 min. The resulting slides were exposed to a solution of $NaCNBH_3$ (66×10^{-3} M in PBS) to reduce the imine bonds formed to more stable amine bonds. The slides were then rinsed with an aqueous 0.4% SDS solution, followed by deionized H_2O. To prevent background cell binding, the substrates were blocked with a solution of 1% bovine serum albumin in PBS for 15 min before use. Then, the suspension of DNA1-linked cells at TA–Fe^{3+} was incubated with the DNA2-modified substrate in pH 7.0 Dulbecco's phosphate-buffered saline. The unbound cells were gently removed from the coatings by rinsing with buffer for 1 min. Cells were viewed using an Olympus BX-51 optical system microscope (Tokyo, Japan) with a blue filter.

Disassembly Experiments: The disassembly of shell was carried out in PBS buffer solutions with different pH values (7.0, 5.0, and 4.0). The effect of EDTA on the shell disassembly was also studied by addition of 10 μL of 7.5×10^{-3} M EDTA into the buffer solution pH 7.0 and pH 5.0. The coated cells were added to the buffer solution and then constantly incubated on a thermostated shaker at 30 °C. After that, the cells were collected by centrifugation. The surface morphology, division condition, and the viability of shell-removed cells were characterized as described above. The cells with or without stimuli were also cultured on the yeast–extract–peptone–dextrose (YPD) agar plate by the spread plate method. After incubation at 30 °C overnight, the number of the bacteria colonies on each plate was observed.

Encapsulation of E. coil Cells with TA–Fe^{3+}: Monocolony of *E. coli* cells on the solid Luria–Bertani (LB) agar plate was transferred to 20 mL of liquid LB culture medium and grown at 37 °C for 12 h under 180 rpm rotation. Then, yeast cells were harvested in 1.5 mL centrifuge tubes by centrifugation and washed three times in 0.85% aqueous NaCl solution. The *E. coil* cells were successively incubated with 0.5 mmol L^{-1} $FeCl_3{\cdot}6H_2O$ and 0.25 mmol L^{-1} TA for 30 s. After centrifugation and wash, the *E. coil* cells at TA–Fe^{3+} were obtained. The viability of the noncoated and coated bacteria was assessed with live/dead assay as described above. For expression of fluorescent protein, the *E. coil* cells were cultured in the presence of galactose instead of glucose for 3 h. The cells were then imaged with Olympus BX-51 optical system microscope. For quantitative study of the expressed fluorescence protein, the flow cytometric analysis was performed on BD FACS Aria. The excitation wavelength was 488 nm and signals were collected at FITC channel 500–560 nm.

Encapsulation of PC12 Cells with TA–Fe^{3}: PC12 cells (rat pheochromocytoma, American Type Culture Collection) were cultured in DMEM (Gibco BRL) medium supplemented with 5% fetal bovine serum, 10% horse serum in a 5% CO_2 humidified environment at 37 °C. When the cells were grown to 70%–80% confluency, they were detached from the flask by trypsin. The cells were collected by centrifugation and then washed with 0.85% aqueous NaCl solution twice. After the sequential addition of TA and $FeCl_3$ solution, the cell suspension was mixed and centrifuged to obtain the PC12 cells at TA–Fe^{3+}. The viability of cells was assayed with live/dead cell staining. For this, the PI and AM dyes were added to the cells. After 15 min incubation, the cells were imaged under the microscope.

Supporting Information

Supporting Information is available from the Wiley Online Library or from the author.

Acknowledgements

This work was supported by 973 Project (2011CB936004, 2012CB720602), and NSFC (21210002, 21431007, 91413111).

Received: January 5, 2015
Revised: March 30, 2015
Published online: May 13, 2015

[1] L. Flintoft, *Nat. Rev. Microbiol.* **2003**, *1*, 88.
[2] K. Birmingham, V. Gradinaru, P. Anikeeva, W. M. Grill, V. Pikov, B. McLaughlin, P. Pasricha, D. Weber, K. Ludwig, K. Famm, *Nat. Rev. Drug. Discovery* **2014**, *13*, 399.
[3] S. A. Morin, R. F. Shepherd, S. W. Kwok, A. A. Stokes, A. Nemiroski, G. M. Whitesides, *Science* **2012**, *337*, 828.
[4] Q. Liu, C. Wu, H. Cai, N. Hu, J. Zhou, P. Wang, *Chem. Rev.* **2014**, *114*, 6423.
[5] Y. Tang, C. Zhang, J. Wang, X. Lin, L. Zhang, Y. Yang, Y. Wang, Z. Zhang, J. W. M. Bulte, G.-Y. Yang, *Adv. Funct. Mater.* **2015**, *25*, 1024.
[6] C. Ricordi, T. B. Strom, *Nat. Rev. Immunol.* **2004**, *4*, 258.
[7] V. Kozlovskaya, O. Zavgorodnya, Y. Chen, K. Ellis, H. M. Tse, W. X. Cui, J. A. Thompson, E. Kharlampieva, *Adv. Funct. Mater.* **2012**, *22*, 3389.
[8] G. C. Wang, R. Y. Cao, R. Chen, L. J. Mo, J. F. Han, X. Y. Wang, X. R. Xu, T. Jiang, Y. Q. Deng, K. Lyu, S. Y. Zhu, E. D. Qin, R. K. Tang, C. F. Qin, *Proc. Natl. Acad. Sci. U.S.A.* **2013**, *110*, 7619.
[9] G. Wang, X. Li, L. Mo, Z. Song, W. Chen, Y. Deng, H. Zhao, E. Qin, C. Qin, R. Tang, *Angew. Chem. Int. Ed.* **2012**, *51*, 10576.
[10] J. T. Wilson, W. X. Cui, V. Kozovskaya, E. Kharlampieva, D. Pan, Z. Qu, V. R. Krishnamurthy, J. Mets, V. Kumar, J. Wen, Y. H. Song, V. V. Tsukruk, E. L. Chaikof', *J. Am. Chem. Soc.* **2011**, *133*, 7054.
[11] X. L. Xiong, H. P. Liu, Z. L. Zhao, M. B. Altman, D. Lopez-Colon, C. J. Yang, L. J. Chang, C. Liu, W. H. Tan, *Angew. Chem. Int. Ed.* **2013**, *52*, 1472.
[12] S. H. Yang, S. M. Kang, K. B. Lee, T. D. Chung, H. Lee, I. S. Choi, *J. Am. Chem. Soc.* **2011**, *133*, 2795.
[13] M. X. You, Y. Chen, L. Peng, D. Han, B. C. Yin, B. C. Ye, W. H. Tan, *Chem. Sci.* **2011**, *2*, 1003.
[14] R. F. Fakhrullin, A. I. Zamaleeva, R. T. Minullina, S. A. Konnova, V. N. Paunov, *Chem. Soc. Rev.* **2012**, *41*, 4189.
[15] R. Kempaiah, A. Chung, V. Maheshwari, *ACS Nano* **2011**, *5*, 6025.
[16] M. Martin, F. Carmona, R. Cuesta, D. Rondon, N. Galvez, J. M. Dominguez-Vera, *Adv. Funct. Mater.* **2014**, *24*, 3489.
[17] B. Wang, G. Wang, B. Zhao, J. Chen, X. Zhang, R. Tang, *Chem. Sci.* **2014**, *5*, 3463.
[18] I. Drachuk, M. K. Gupta, V. V. Tsukruk, *Adv. Funct. Mater.* **2013**, *23*, 4437.
[19] R. A. Chandra, E. S. Douglas, R. A. Mathies, C. R. Bertozzi, M. B. Francis, *Angew. Chem. Int. Ed.* **2006**, *45*, 896.
[20] D. Rabuka, M. B. Forstner, J. T. Groves, C. R. Bertozzi, *J. Am. Chem. Soc.* **2008**, *130*, 5947.
[21] L. Lybaert, E. De Vlieghere, R. De Rycke, N. Vanparijs, O. De Wever, S. De Koker, B. G. De Geest, *Adv. Funct. Mater.* **2014**, *24*, 7139.
[22] K. Gabrielse, A. Gangar, N. Kumar, J. C. Lee, A. Fegan, J. J. Shen, Q. Li, D. Vallera, C. R. Wagner, *Angew. Chem. Int. Ed.* **2014**, *53*, 5112.
[23] X. Hou, H. C. Zhang, L. Jiang, *Angew. Chem. Int. Ed.* **2012**, *51*, 5296.
[24] L. Zhang, J. Wu, Y. Wang, Y. Long, N. Zhao, J. Xu, *J. Am. Chem. Soc.* **2012**, *134*, 9879.
[25] X. Yao, Y. L. Song, L. Jiang, *Adv. Mater.* **2011**, *23*, 719.
[26] J. Heo, T. Kang, S. G. Jang, D. S. Hwang, J. M. Spruell, K. L. Killops, J. H. Waite, C. J. Hawker, *J. Am. Chem. Soc.* **2012**, *134*, 20139.
[27] A. M. Spokoyny, D. Kim, A. Sumrein, C. A. Mirkin, *Chem. Soc. Rev.* **2009**, *38*, 1218.
[28] O. K. Farha, A. O. Yazaydin, I. Eryazici, C. D. Malliakas, B. G. Hauser, M. G. Kanatzidis, S. T. Nguyen, R. Q. Snurr, J. T. Hupp, *Nat. Chem.* **2010**, *2*, 944.
[29] J. H. Park, K. Kim, J. Lee, J. Y. Choi, D. Hong, S. H. Yang, F. Caruso, Y. Lee, I. S. Choi, *Angew. Chem. Int. Ed.* **2014**, *53*, 12420.
[30] J. Liu, S. Chakraborty, P. Hosseinzadeh, Y. Yu, S. Tian, I. Petrik, A. Bhagi, Y. Lu, *Chem. Rev.* **2014**, *114*, 4366.
[31] J. Guo, Y. Ping, H. Ejima, K. Alt, M. Meissner, J. J. Richardson, Y. Yan, K. Peter, D. von Elverfeldt, C. E. Hagemeyer, F. Caruso, *Angew. Chem. Int. Ed.* **2014**, *53*, 5546.
[32] K. L. Haas, K. J. Franz, *Chem. Rev.* **2009**, *109*, 4921.
[33] S. W. Werneke, C. Swann, L. A. Farquharson, K. S. Hamilton, A. M. Smith, *J. Exp. Bot.* **2007**, *210*, 2137.
[34] C. C. Broomell, M. A. Mattoni, F. W. Zok, J. H. Waite, *J. Exp. Bot.* **2006**, *209*, 3219.
[35] M. J. Sever, J. T. Weisser, J. Monahan, S. Srinivasan, J. J. Wilker, *Angew. Chem.* **2004**, *43*, 448.
[36] M. J. Harrington, A. Masic, N. Holten-Andersen, J. H. Waite, P. Fratzl, *Science* **2010**, *328*, 216.
[37] S. M. Lee, E. Pippel, U. Gosele, C. Dresbach, Y. Qin, C. V. Chandran, T. Brauniger, G. Hause, M. Knez, *Science* **2009**, *324*, 488.
[38] T. S. Sileika, D. G. Barrett, R. Zhang, K. H. A. Lau, P. B. Messersmith, *Angew. Chem. Int. Ed.* **2013**, *52*, 10766.
[39] S. Quideau, D. Deffieux, C. Douat-Casassus, L. Pouysegu, *Angew. Chem. Int. Ed.* **2011**, *50*, 586.
[40] H. Lee, S. M. Dellatore, W. M. Miller, P. B. Messersmith, *Science* **2007**, *318*, 426.
[41] D. R. Dreyer, D. J. Miller, B. D. Freeman, D. R. Paul, C. W. Bielawski, *Chem. Sci.* **2013**, *4*, 3796.
[42] H. O. Ham, Z. Q. Liu, K. H. A. Lau, H. Lee, P. B. Messersmith, *Angew. Chem. Int. Ed.* **2011**, *50*, 732.
[43] J. J. T. M. Swartjes, T. Das, S. Sharifi, G. Subbiahdoss, P. K. Sharma, B. P. Krom, H. J. Busscher, H. C. van der Mei, *Adv. Funct. Mater.* **2013**, *23*, 2843.
[44] S. M. Kang, S. Park, D. Kim, S. Y. Park, R. S. Ruoff, H. Lee, *Adv. Funct. Mater.* **2011**, *21*, 108.
[45] N. Holten-Andersen, M. J. Harrington, H. Birkedal, B. P. Lee, P. B. Messersmith, K. Y. C. Lee, J. H. Waite, *Proc. Natl. Acad. Sci. U.S.A.* **2011**, *108*, 2651.
[46] J. Sedo, J. Saiz-Poseu, F. Busque, D. Ruiz-Molina, *Adv. Mater.* **2013**, *25*, 653.
[47] M. Krogsgaard, A. Andersen, H. Birkedal, *Chem. Commun.* **2014**, *50*, 13278.
[48] H. Ejima, J. J. Richardson, K. Liang, J. P. Best, M. P. van Koeverden, G. K. Such, J. W. Cui, F. Caruso, *Science* **2013**, *341*, 154.
[49] B. Wang, P. Liu, W. G. Jiang, H. H. Pan, X. R. Xu, R. K. Tang, *Angew. Chem. Int. Ed.* **2008**, *47*, 3560.
[50] I. Drachuk, O. Shchepelina, S. Harbaugh, N. Kelley-Loughnane, M. Stone, V. V. Tsukruk, *Small* **2013**, *9*, 3128.
[51] J. Xie, K. Chen, H. Y. Lee, C. J. Xu, A. R. Hsu, S. Peng, X. Y. Chen, S. H. Sun, *J. Am. Chem. Soc.* **2008**, *130*, 7542.
[52] Y. Liu, T. Chen, C. Wu, L. Qiu, R. Hu, J. Li, S. Cansiz, L. Zhang, C. Cui, G. Zhu, M. You, T. Zhang, W. Tan, *J. Am. Chem. Soc.* **2014**, *136*, 12552.
[53] M. Miljevic, B. Geiseler, T. Bergfeldt, P. Bockstaller, L. Fruk, *Adv. Funct. Mater.* **2014**, *24*, 907.
[54] M. Li, Z. Liu, J. S. Ren, X. G. Qu, *Chem. Sci.* **2012**, *3*, 868.

[55] M. Mahmoudi, H. Hosseinkhani, M. Hosseinkhani, S. Boutry, A. Simchi, W. S. Journeay, K. Subramani, S. Laurent, *Chem. Rev.* **2010**, *111*, 253.
[56] M. M. Britton, *Chem. Soc. Rev.* **2010**, *39*, 4036.
[57] K. Glunde, D. Artemov, M.-F. Penet, M. A. Jacobs, Z. M. Bhujwalla, *Chem. Rev.* **2010**, *110*, 3043.
[58] F. Wang, X. Liu, *Chem. Soc. Rev.* **2009**, *38*, 976.
[59] R. F. Fakhrullin, L. V. Shlykova, A. I. Zamaleeva, D. K. Nurgaliev, Y. N. Osin, J. Garcia-Alonso, V. N. Paunov, *Macromol. Biosci.* **2010**, *10*, 1257.
[60] A. A. Twite, S. C. Hsiao, H. Onoe, R. A. Mathies, M. B. Francis, *Adv. Mater.* **2012**, *24*, 2380.